JACS
JOURNAL OF THE AMERICAN CHEMICAL SOCIETY

Article

pubs.acs.org/JACS

Thermally-Induced Phase Transition of Pseudorotaxane Crystals: Changes in Conformation and Interaction of the Molecules and Optical Properties of the Crystals

Masaki Horie,*[,†] Yuji Suzaki,[‡] Daisuke Hashizume,[§] Tomoko Abe,[‡] Tiendi Wu,[†] Takafumi Sassa,[∥] Takuya Hosokai,[⊥] and Kohtaro Osakada[‡]

[†]Department of Chemical Engineering, Frontier Research Center on Fundamental and Applied Sciences of Matters, National Tsing Hua University, 101, Sec. 2, Kuang-Fu Road, Hsinchu 30013, Taiwan

[‡]Chemical Resources Laboratory, Tokyo Institute of Technology, 4259 Nagatsuta, Midori-ku, Yokohama 226-8503, Japan

[§]Advanced Technology Support Division and [∥]Flucto-Order Functions Research Team, RIKEN Advanced Science Institute, 2-1 Hirosawa, Wako, Saitama 351-0198, Japan

[⊥]Department of Materials Science and Engineering, Iwate University, Ueda 4-3-5, Morioka 020-8551, Japan

Supporting Information

ABSTRACT: This paper presents a pseudorotaxane that acts as a thermally driven molecular switch in the single-crystal state. Crystals of the cationic pseudorotaxane consisting of dibenzo[24]crown-8 (DB24C8) and *N*-(xylylammonium)-methylferrocene as the cyclic and axle component molecules, respectively, undergo crystalline-phase transition at 128 °C with heating and 116 °C with cooling, according to differential-scanning-calorimetry measurements. X-ray crystallographic analyses revealed that the phase transition was accompanied by rotation of the 4-methylphenyl group of the axle component molecule and a simultaneous shift in the position of the PF_6^- counteranion. Crystalline phase transition changes the conformation and position of the DB24C8 molecule relative to the ammonium cation partially; the interaction between the cyclic component and the PF_6^- anion in the crystal changes to a greater extent. Moreover, there are changes in the vibration angle (θ) and birefringence (Δn) on the (001) face of the crystal transitionally; θ is rotated by +12°, and Δn is decreased from 0.070 to 0.059 upon heating across the phase transition temperature. The phase transition and accompanying change in the optical properties of the crystal occur reversibly and repeatedly upon heating and cooling processes. The switching rotation of the aromatic plane of the molecule induces a change in the optical anisotropy of the crystal, which is regarded as a demonstration of a new type of optical crystal. Partial replacement of the PF_6^- anion with the bulkier AsF_6^- anion forms crystals with similar crystallographic parameters. An increase in the AsF_6^- content decreases the reversible-phase-transition temperature gradually down to 99 °C (T_{end}) and 68 °C (T_{exo}) ([AsF_6^-]:[PF_6^-] = 0.4:0.6).

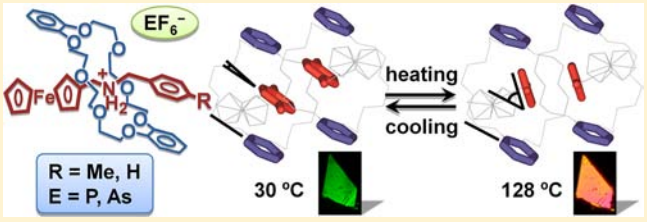

INTRODUCTION

Molecular and supermolecular systems that undergo structural changes upon external stimulation can potentially be applied as nanosize components of opto-electronics.[1−5] Rotaxanes and pseudorotaxanes, which are composed of interlocked ring and axle molecules, have been important molecules exhibiting such functions[6−9] since the discovery of molecular shuttles based on their unique switching behavior.[6a,b] Sliding of macrocycle between the stations along the axle component causes a distinct structural change from one metastable state to the other. On the basis of this concept, molecules that cause shuttling of the macrocycle upon an external stimulus have been achieved by designing the cyclic component with stations for the functional group of the axle component.[6−8] This motion of rotaxanes has been observed in solution in many cases, but it occurs isotropically in solution from a macroscopic viewpoint. On the other hand, the operations of rotaxanes with an ordered direction in the solid state provide regulated molecular motions, which are required for efficient molecular devices. Several research groups have achieved concerted motion of rotaxanes with high orientation using rotaxane films supported on a solid surface; moreover, these groups have exhibited a unique performance of the surface due to external stimulation.[10−12] Shuttling of rotaxanes in monolayer films can bend the cantilever of an atomic force microscope, thereby forming an artificial molecular muscle;[10] it can control the electrical conductivity, thereby forming a high-density molecular memory on a crossed electrode.[11] In addition, this shuttling could

Received: May 11, 2012
Published: October 6, 2012

   dx.doi.org/10.1021/ja304406c | J. Am. Chem. Soc. 2012, 134, 17932−17944

Scheme 1. Pseudorotaxane Formation

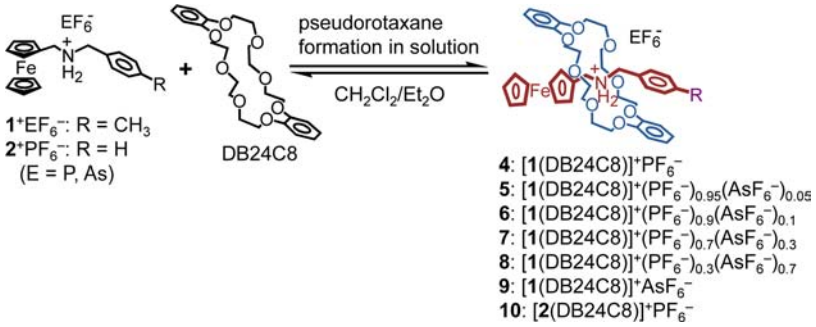

transport a droplet of diiodomethane on a monolayer surface under photoirradiation.[12]

Single crystals of organic compounds consist of molecules packed with a high order of molecular alignment owing to the crystallographic symmetry, and the molecular motion in the crystal is restricted by limitations in space around the molecule. Despite this restriction, the crystals allow rapid motion of the molecules and supermolecules within them.[13−15] Metal organic frameworks (MOFs) have recently been applied with rotaxanes and catenanes to introduce dynamics in the rigid MOF, in which flexible interlocked components allow movements in the MOF backbone.[14] Garcia-Garibay and co-workers reported a single-crystalline molecular gyroscope consisting of *p*-diethynylphenylene molecules that are connected to trityl groups, which was developed by surrounding the rotational axle with bulky trityl groups to create a free volume.[15] Nakamura and co-workers reported the rotational motion of an anilinium axle surrounded by a crown ether with switchable magnetic properties in the single-crystal state due to the Ni complex with a 2-thioxo-1,3-dithiole-4,5-dithiolate ligand.[16] These results suggest that rotation of the axle and cyclic molecules may occur even in the crystal state. Consequently, rotaxanes and pseudorotaxanes in the crystals can undergo rotation of the cyclic and/or axle component. Few reports, however, have appeared in the literature related to the performance of single-crystalline molecular switches composed of rotaxanes.[14a,b]

We have reported that the crystal structure of a pseudorotaxane can be manipulated by thermal stimulation, allowing possible integration into a preliminary form of a molecular switches.[17] Further studies revealed that the change in the crystalline structure of the pseudorotaxane involved a major shift in the PF_6^- counteranion as well as its interaction with the dibenzo[24]crown-8 (DB24C8) molecules. Here we report the full details of our studies of pseudorotaxane crystals, including the results of accurate determination of the first-order solid-to-solid phase transition by a pseudorotaxane crystal using X-ray crystallography as well as the induced change in the optical anisotropy of the crystals.

RESULTS AND DISCUSSIONS

Crystalline-Phase Transition of the Pseudorotaxane. Scheme 1 summarizes the unique features of the pseudorotaxanes examined in this study. We selected dialkylammonium containing 4-methylphenyl and ferrocenyl terminal groups, *N*-(xylylammonium)methylferrocene (1^+) as the axle cation and DB24C8 as the cyclic molecule to form [2]pseudorotaxanes **4**−**9**, which have various molar ratios of counteranions PF_6^- and AsF_6^-, as shown in Scheme 1. Since these two anions have similar structure and different size (P < As), the cationic pseudorotaxanes with the counteranions as well as with their mixtures would form the isomorphous crystals. In addition, *N*-(benzylammonium)methylferrocene (2^+) and *N*-(ethylammonium)methylferrocene (3^+) were used to prepare [2]pseudorotaxanes **10** and **11**, respectively (Schemes 1 and 2).

Scheme 2. Pseudorotaxane Formation

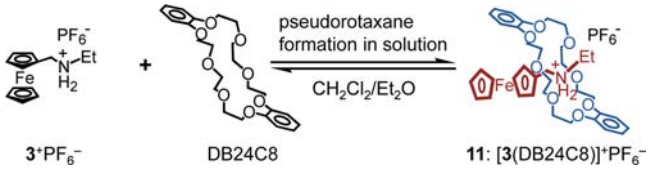

In a solution, reversible formation and dissociation of the pseudorotaxanes yielded a mixture containing pseudorotaxanes and the free components.[9] Recrystallization from solution by diffusion of Et_2O into the CH_2Cl_2 solution caused self-assembly of the pseudorotaxanes and formation of their single crystals. In the crystals of **4**−**8**, a pair of pseudorotaxanes exhibits intermolecular $\pi-\pi$ stacking between the tolyl end groups of the axle component in a unit cell at low temperature (room temperature or −150 °C) (Scheme 3a). Heating of the crystals

Scheme 3. Schematic of Molecular Alignment in the Crystal State: (a) 4−8 at Room Temperature, π-Stacked Tolyl Ends Parallel to the Aromatic Planes of the Macrocycle; (b) 4−7 of High Temperature Phase, π-Stacked Tolyl Ends Inclined to the Aromatic Planes of the Macrocycle

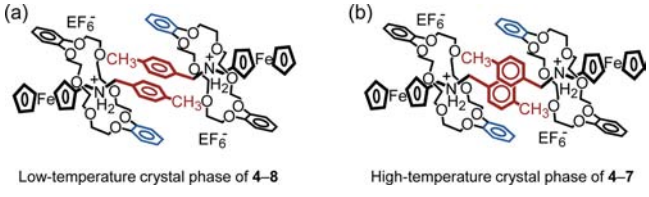

of **4**−**7** causes simultaneous rotations of the aromatic rings of the two axle component molecules, in which the tolyl ends incline to the aromatic plane of the macrocyclic component (Scheme 3b). However, pseudorotaxane **8** composed of DB24C8 with $1^+(PF_6^-)_{0.3}(AsF_6^-)_{0.7}$ does not show such a structural change upon heating. Pseudorotaxanes **9** and **10** formed from the reaction of DB24C8 with $1^+AsF_6^-$ and with $2^+PF_6^-$ are also obtained as single crystals, but their conformation at room temperature is similar to that of **4**−**7** in the crystals at high temperature (Scheme 3b). The above structural change of **4**−**7** in the crystals takes places reversibly depending on the temperature. It corresponds to the crystal-to-

dx.doi.org/10.1021/ja304406c | J. Am. Chem. Soc. 2012, 134, 17932−17944

crystal phase transition, which acts as a molecular switch controlling the anisotropic properties of the crystals, as described below in detail.

Differential scanning calorimetry (DSC) of the crystalline **4** ([**1**(DB24C8)]$^+PF_6^-$) revealed endothermic (128 °C) and exothermic (116 °C) peaks, as shown in Figure 1a. The

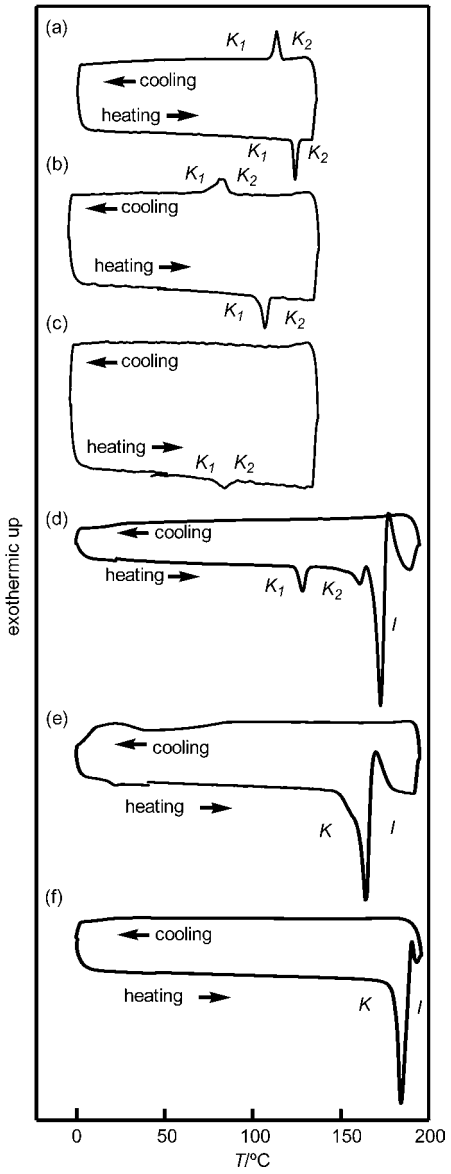

Figure 1. DSC heating and cooling scans of (a) **4**, (b) **7**, and (c) **8** at 2 °C min^{-1} up to 130 °C and (d) **4**, (e) **9**, and (f) **10** at 5 °C min^{-1} up to 190 °C. Symbols: *K*, crystal; *I*, isotropic.

thermodynamic parameters are determined to be ΔH = 7.6 kJ mol^{-1} and ΔS = 19 J mol^{-1} K^{-1}. DSC of fine crystals of **5**–**7** measured up to 130 °C also showed reversible endo- and exothermic peaks (Figure 1b for **7**) derived from the crystal-to-crystal phase transition. These peak positions, T_{end} and T_{exo}, are plotted with the fraction of the counteranions [AsF_6^-]/[(AsF_6^-) + (PF_6^-)] in Figure 2. As the fraction of AsF_6^- increases, the endothermic peak of the phase transition (Figure 2a) is shifted to lower temperatures from 128 °C for **4** (PF_6^- only) to 86 °C at an AsF_6^- fraction of 0.6. The plots for the exothermic peaks (Figure 2b) show a similar trend; the peak

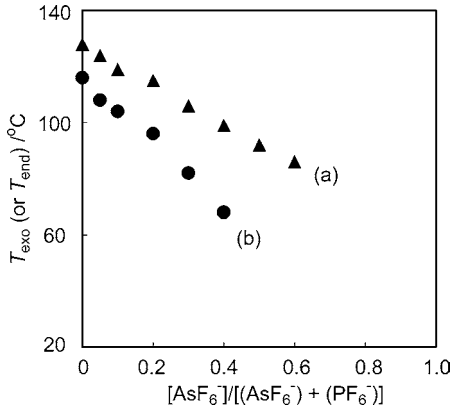

Figure 2. Crystal-to-crystal phase transition temperatures vs ratio of counteranions PF_6^- and AsF_6^-. Temperature of (a) endothermic peak (T_{end}) upon heating (triangles) and (b) exothermic peak (T_{exo}) upon cooling (circles).

shifts from 115 °C for **4** to 68 °C at an AsF_6^- fraction of 0.4. Pseudorotaxanes with a higher AsF_6^- fraction than 0.6 exhibited a significant decrease in the peak intensity along with degradation of reversibility (Figure 1c), and eventually these peaks were disappeared in DSC of an AsF_6^- fraction of 0.7 (**8**). When **4** was scanned up to a higher temperature (190 °C), irreversible endothermic peaks appeared at 150 and 170 °C, and the latter peak, which has a large ΔH (46 kJ mol^{-1}) and large ΔS (105 J mol^{-1} K^{-1}), is assigned to the melting, which was confirmed using optical microscopy with a hot stage. Recooling the once-heated crystals above 170 °C did not yield any exothermic peaks (Figure 1d). The pseudorotaxanes show different thermal behaviors from the axle molecule **1**, which show an irreversible endothermic peak at 188 °C, and from DB24C8, which shows melting (T_{end} = 104 °C, T_{exo} = 79 °C). A vacuum-deposition film obtained from a melted crystal of **4** was identical to that of DB24C8 because **4** is converted into the cyclic and axle components above the melting point (170 °C) owing to an entropic deficit (see Figure S1 in the Supporting Information). Compounds **9** and **10** have the same crystallographic structure as that of high temperature phase of **4**–**7** (Scheme 2b), and cause only melting at 164 and 170 °C, respectively, upon heating (Figure 1e,f). Crystals of compound **11**, having an ethyl terminal group of the axle molecule, did not show any DSC peak below 130 °C (Figure S2j in the Supporting Information). Thus, crystals of **4**–**7** exhibit thermally induced phase transition whose temperature is shifted to lower temperature as increase of portion of AsF_6^- in the anions. Extrapolation of plots of Figure 2 seems to suggest that crystals of the pseudorotaxane containing AsF_6^- only can have a similar structure to the high temperature phase of **4**. In fact, results of the X-ray analysis of **9** showed the structure in Scheme 3b.

The IR spectra of **4** measured at 30 and 100 °C showed a peak due to N–H vibration at 3185 cm^{-1} (Figure S3 in the Supporting Information). Heating the sample to 128 °C shifted the peak to a lower wavenumber (3162 cm^{-1}). The peak shift corresponds to a decrease in the vibration energy of the two N–H bonds by 0.55 kJ mol^{-1}. These results indicate weakening of the N–H bonds in the high-temperature crystalline phase, which is probably the result of an increase in the strength of the N–H···O hydrogen bond (vide infra).

The above DSC and IR results suggest that pseudorotaxane **4** changes structure in the crystalline state upon heating to 128

dx.doi.org/10.1021/ja304406c | J. Am. Chem. Soc. 2012, 134, 17932–17944

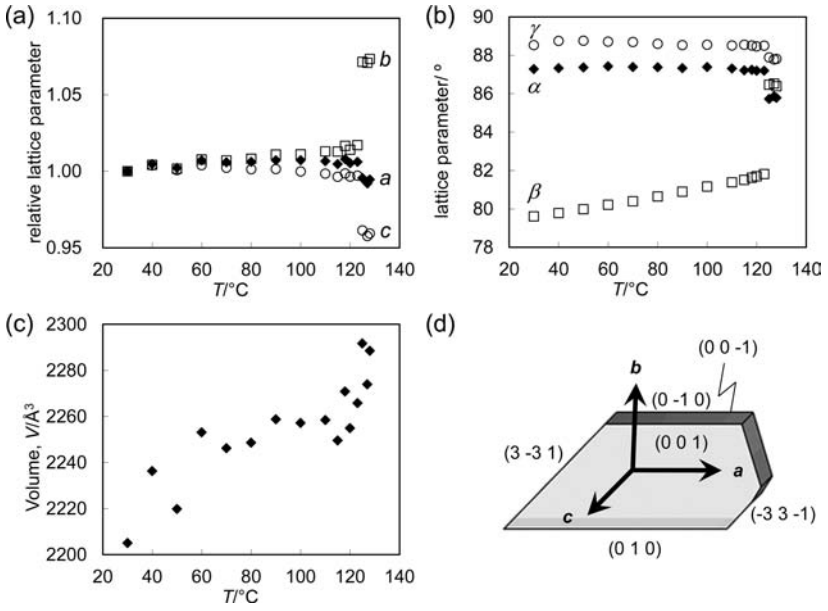

Figure 3. Temperature dependence of lattice parameters of **4**. (a) *a*, *b*, *c*, (b) *α*, *β*, *γ*, (c) volume *V*, and (d) axes superimposed on the crystal habitus.

°C. The small ΔH value (7.6 kJ mol^{-1}) of the reversible phase transition of **4** corresponds to a crystalline-phase transition accompanied by a conformational change in the molecule rather than cleavage of a covalent bond. Consequently, detailed X-ray crystallographic measurements of single crystals of **4** were made at various temperatures (from −150 to 128 °C). Figure 3 plots the change in the lattice parameters (*a*, *b*, *c*, *α*, *β*, *γ*, and *V*). In the range between −150 and 128 °C, the crystals keep the single-crystal form with a triclinic system ($P\bar{1}$, $Z = 2$). The cell constants changed to a small degree below the phase transition temperature (128 °C), whereas significant changes were noted in the length of the *b* and *c* axes (ca. +7% and −4%, respectively) and in the angles of *β* [81.024(7)° and 86.50(3)°] at 128 °C (Figure 3 and Table S1 in the Supporting Information).

Figure 4 shows the crystal structures of **4** at −150 and 128 °C. Detailed data on the bond distances and angles are summarized in Tables 1−3. The interlocked structure of the pseudorotaxanes is retained at both temperatures. The macrocyclic component is associated with the axle component by N−H···O hydrogen bonds as well as C−H···*π* attractive interactions between a cyclopentadienyl (Cp) group and the catechol ring (Figure 4a). This conformational structure of the pseudorotaxane and interaction between the cyclic and axle components are similar at temperatures of −150, 30, and 100 °C. The structure at 128 °C, however, shows slight change of the interaction between the NH_2 group of the axle component and DB24C8 (Figure 4b). Close contact for O1···H2 (2.35 Å) at −150 °C becomes less significant at 128 °C (2.76 Å) (Table 3). The results together with change of the O1···H−C contact between the high and low temperature phases are ascribed to slight change of conformation of DB24C8. The ferrocenyl group of the axle molecule and the catechol ring of DB24C8 exhibit a C(Cp)−H···*π* attractive interaction and a negligible change in their relative positions due to the phase transition. The C(Cp)−CH_2−NH_2−CH_2−C(tolyl) chain of **4** has an *all-anti* conformation in the single crystal. The dihedral angles of C(Cp)−CH_2−NH_2−CH_2 and CH_2−NH_2−CH_2−C(tolyl) are 171, 169° and 174, 178° before and after the phase transition, respectively. More striking change is observed in 4-methyl-

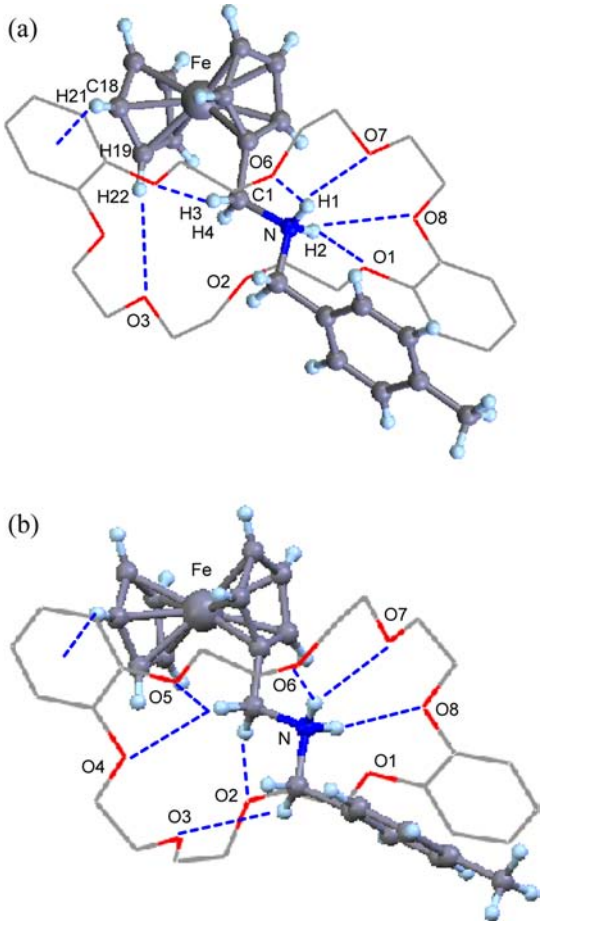

Figure 4. Molecular structures of **4** at (a) −150 °C and (b) 128 °C. A few of the hydrogen atoms and PF_6^- counteranions were omitted for simplicity. Blue-dotted lines indicate geometric contacts between atoms.

phenyl terminal group of the axle molecule; the aromatic plane is rotated by 37° on heating at 128 °C.

dx.doi.org/10.1021/ja304406c | J. Am. Chem. Soc. 2012, 134, 17932−17944

Table 1. Distances and Angles of the Crystal Structure of 4

	distances between F and H	angles
P1−F1···H42*	2.59 Å	126°
P1−F1···H52*	2.67 Å	108°
P1−F2···H31*	2.62 Å	104°
P1−F2···H38	2.65 Å	130°
P1−F3···H28	2.53 Å	102°
P1−F3···H31	2.52 Å	108°
P1−F3···H51*	2.62 Å	124°
P1−F4···H54*	2.62 Å	132°
P1−F5···H35*	2.64 Å	124°
P1−F5···H44*	2.47 Å	106°
P1−F5···H47*	2.53 Å	111°
P1−F6···H38	2.63 Å	133°

Table 2. Distances and Angles of 4[a]

	distances/angles at −150 °C	distances/angles at 128 °C
Ring A−Ring B	3.71 Å/6.2°	4.69 Å/45.1°
Ring A−Ring C	9.35 Å/3.6°	8.78 Å/53.0°
Ring B−Ring C	11.39 Å/3.6°	10.96 Å/9.8°
Ring C−Cp	5.14 Å/88.0°	5.07 Å/90.0°
Ring A−Ring A′	3.83 Å/0°	3.81 Å/0°
Ring B−Ring B′	10.23 Å/0°	10.96 Å/0°
PF_6−(PF_6) ′	11.05 Å	11.92 Å
PF_6−(PF_6) ″	10.19 Å	10.22 Å
PF_6−Ring B	6.20 Å	7.11 Å
(PF_6)′−Ring B	6.65 Å	6.36 Å
N−Ring A	3.74 Å	3.71 Å
N−Ring B	5.09 Å	5.06 Å
N−Ring C	6.33 Å	6.00 Å
N−Fe	4.37 Å	4.39 Å

[a]Distances involving the rings, **A**, **B**, and **C**, indicate the distance from the centroid of the ring.

Figure 5a,b compares the total structures of a pair of **4** and structural relationship of its aromatic planes in the crystals. At −150 °C, aromatic planes of the two neighboring axle components, **A** and **A**′, as well as close catechol planes of the DB24C8, **B** and **B**′, are arranged in a parallel fashion because of $\pi-\pi$ stacking interactions between the neighboring planes. Heating the crystals at 128 °C causes rotation of the aromatic rings of the axle components, whereas those of the macrocycle do not change their orientation. Thus, a pair of rings, **A** and **A**′, of two axle molecules are inclined to the catechol planes **B** and **B**′, thereby forming a new conformation stabilized by C−H···π interactions between rings **A** and **B** as well as **A**′ and **B**′. The angles and distances between rings **A** and **B** change from 6° to 45° and 3.71 to 4.69 Å, respectively (Table 2). A crystallographic point of symmetry between two pseudorotaxanes (Figures 5a and 5b) exists in a unit cell; therefore, the aromatic ring **A** is rotated to the same degrees as **A**′ at the phase transition temperature.

Figure 6 shows crystal packing of pseudorotaxane **4** at −150 and 128 °C. At low temperature, the PF_6^- anion is surrounded by four cationic pseudorotaxanes $[\mathbf{1}(DB24C8)]^+$ in the crystal, and it has close contacts with the CH_2 groups of the DB24C8 component (Figure 6a). There are 12 geometric contacts between F and the hydrogens of DB24C8 within the sum of the van der Waals' radius of F and H (<2.67 Å) at −150 °C, which indicates the presence of multiple P−F···H−C hydrogen bonds (Table 1). These geometrical contacts between PF_6^- and DB24C8 become negligible at 128 °C in the crystals, in which the distances between F and H atoms are longer than 2.73 Å (e.g., F3 and H23 in Figure 6b). The distance between the P atom of PF_6^- and the centroid of ring **B** increased from 6.20 Å (−150 °C) to 7.11 Å (128 °C). These structural changes are related to anisotropic shift of the anions caused by the phase transition. P···P distance between the neighboring PF_6^- along the *b* axis is elongated from 11.05 Å (−150 °C) to 11.92 Å (128 °C), which corresponds to lengthening of the *b* axis. In contrast, the change in distance between the PF_6^- anions is insignificant along the *a* axis (10.19 Å at −150 °C and 10.22 Å at 128 °C). The AsF_6^- anion is bulkier than PF_6^- anion and may form weaker hydrogen bonds with the aliphatic groups of DB24C8 than that of PF_6^- anion.[18] Structural changes of the pseudorotaxanes around the counteranions during the phase transition can be summarized as below. Heating of the crystal of **4** above the phase transition temperature intensively activates the hydrogen bonds between PF_6^- and DB24C8, and removes the anion out of the range of C−H···F hydrogen bonds. This process seems to generate the positive ΔH and ΔS, as observed in DSC. The PF_6^- counteranions then move along the *b* axis, thereby expanding the crystal lattice mainly toward the direction of the *b* axis. The separation of PF_6^- creates a space around the DB24C8 molecules, which allows conformational change of the tolyl group of the pseudorotaxane.

Further comparison of the detailed crystallographic data of the pseudorotaxanes with different counteranions was conducted in order to obtain more insights of the anion effect on the phase transition. Compound **8** with an anion ratio of

Table 3. Distances and Angles of the Crystal Structure of 4[a]

	distances between H and O at −150 °C/the corresponding distances at 128 °C	angles at −150 °C/the corresponding angles at 128 °C
N1−H1···O6	2.29 Å/2.13 Å	128°/153°
N1−H1···O7	2.18 Å/2.27 Å	157°/130°
N1−H2···O1	2.35 Å/(2.76 Å)	163°/(141°)
N1−H2···O8	2.53 Å/2.26 Å	123°/159°
C1−H3···O4	(2.85 Å)/2.68 Å	(133°)/151°
C1−H3···O5	2.54 Å/2.66 Å	167°/149°
C1−H4···O2	2.35 Å/2.33 Å	143°/166°
C2−H6···O3	(3.21 Å)/2.62 Å	(148°)/131°
C19−H22···O3	2.70 Å/(3.55 Å)	167°/(162°)
C18−H22···Centroid of ring **C**	3.09 Å/3.12 Å	156°/152°

[a]Data shown in the parentheses indicate the longer distances than the sum of the van der Waals' radius of H and O (>2.72 Å).

dx.doi.org/10.1021/ja304406c | J. Am. Chem. Soc. 2012, 134, 17932−17944

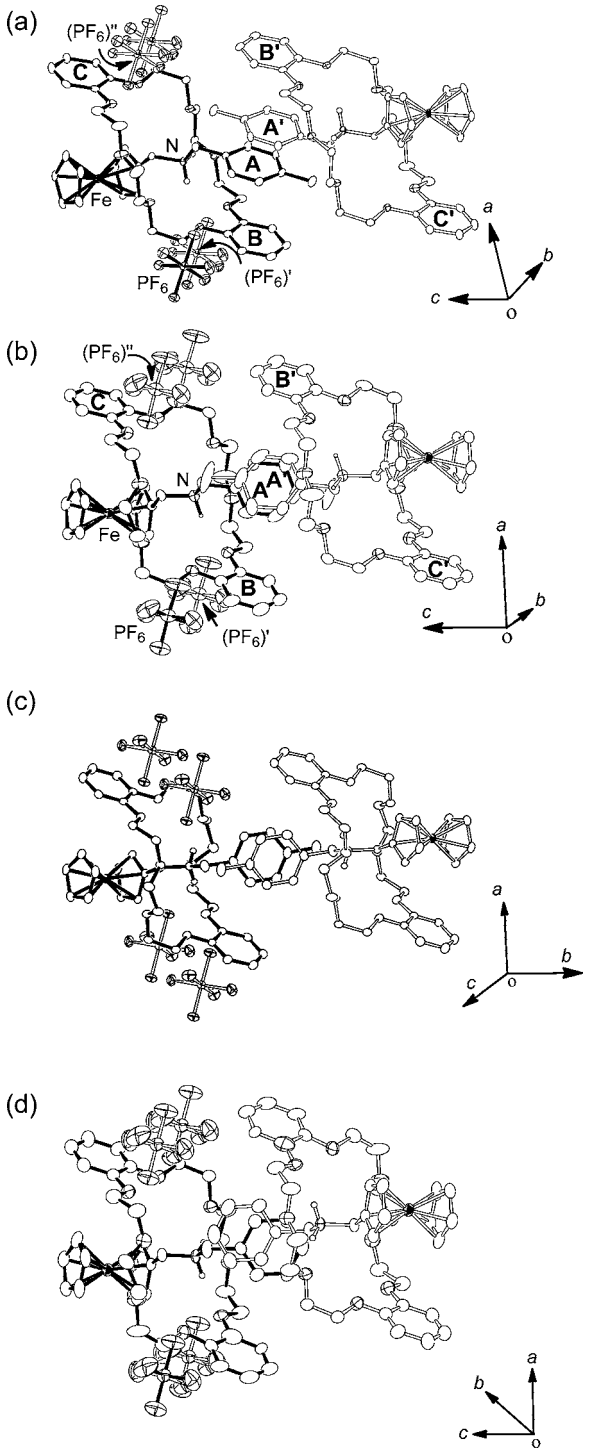

Figure 5. Molecular structures of (a) **4** at −150 °C, (b) **4** at 128 °C, (c) **9** at −150 °C, and (d) **10** at −150 °C.

AsF_6^-/PF_6^- = 7:3 had a quite similar structure to **4**, having PF_6^- exclusively, at −150 °C. The distances between rings **A** and **B** and between rings **A** and **A**′ of **8** are 3.74 and 3.86 Å, respectively, where the corresponding distances of **4** are 3.71 and 3.83 Å (Table 2). Pseudorotaxane **9** with AsF_6^- in the crystals at −150 °C adopts a similar conformation to that of the high-temperature phase of **4** (Figure 5c). As···As distance of the neighboring AsF_6^- anions along the *b* axis of **9** is 11.61 Å at −150 °C, which is comparable with that of the separation of P atom of the PF_6^- anions of **4** in the high-temperature phase (11.92 Å at 128 °C). Thus, AsF_6^- anion of **9** is accommodated in the space among the cationic pseudorotaxanes, which are situated at similar positions of those of high temperature phase of **4** (Scheme 3b). Crystals of **4** at the low temperature phase have close contacts between the fluorine atoms of PF_6^- anion and the C−H groups of DB24C8. The space formed by the cationic pseudorotaxane is too small to contain the AsF_6^- anions which are bulkier than PF_6^-; F−As−F distance in AsF_6^- of **9** (3.45 Å) is significantly longer than the F−P−F distance in PF_6^- of **4** (3.16 Å). Thus, pseudorotaxane **9** does not adopt a crystal structure similar to the low temperature phase of **4** because of steric repulsion between the anion and the cationic pseudorotaxane. Crystals of the mixed anions with the AsF_6^- portion below 0.70 are isomorphous to the low temperature phase of **4**, and those with the As:P ratio below 0.40 exhibit the reversible crystalline phase transition. Increase of AsF_6^- portion probably destabilizes the low temperature phase, and lowers the phase transition temperature, as shown in Figure 2. Apparent decrease of the reaction enthalpy caused by increase of the AsF_6^- portion in the mixed-anion crystals of **5**−**7** can be attributed mainly to relative stability of the low temperature phase.

Macrocyclic DB24C8 of **4** also changes its conformation by the crystal phase transition. Two catechol rings in **4** (rings **B** and **C** in Figure 5) are oriented almost parallel (4°) with a distance of 11.39 Å at −150 °C, and the distance is shortened to 10.96 Å with the angle of 10° at 128 °C. Distance of parallel catechol rings of the neighboring pseudorotaxanes **B** and **B**′ is elongated from 10.23 Å (−150 °C) to 10.96 Å (128 °C) upon heating. Consequently, the space formed by rings **B** and **B**′ is increased by 18% [8.3 $Å^3$ (−150 °C) to 8.9 $Å^3$ (128 °C)]. The phase transition shifts ring **C** closer to the nitrogen atom of the axle molecule [6.33 Å (−150 °C) and 6.00 Å (128 °C)], and ring **B** slightly more remote to the nitrogen [5.09 Å (−150 °C) and 5.06 Å (128 °C)].

The dihedral angles between O−C−C−O in DB24C8 decreased from 77, 70, 74, and 72° at 100 °C to 70, 60, 73, and 71°, respectively, at 128 °C. This indicates that the ethylene glycol chains of DB24C8, which have a contractile structure at low temperature, change to an expanding structure by phase transition. Table 3 summarizes the geometric constants between the hydrogens of the axle component and the oxygens of DB24C8. The distance and angles of $CH_2NH_2CH_2$ hydrogens and the oxygens of DB24C8, shown in Table 3, indicate rearrangement of the hydrogen bonds by phase transition (Figure 4). The average distance between nitrogen and oxygens of DB24C8 is 3.63 Å at −150 °C and 3.48 Å at 128 °C, respectively.

The other outstanding structural change in the phase transition is switching of the conformation of two terminal aryl groups of the axle from those with $\pi-\pi$ interaction to those with C−H···π interaction. A recent theoretical approach showed that the dimerization energy of benzene molecules in the T-shaped configuration with the C−H···π interaction (−10.3 kJ mol^{-1}) and the slipped-parallel configuration with the $\pi-\pi$ stacking interaction (−10.4 kJ mol^{-1}) are almost the same.[19] However, the distances of the centroid of the benzene molecules that minimize the stabilizing energy of these dimers differ; namely, the C−H···π interaction favors longer distances (5.0 Å) than the $\pi-\pi$ stacking interaction (3.9 Å). Consequently, elongation of the interpseudorotaxane distance between catechol rings **B** and **B**′, caused by the anion shift and conformation change of DB24C8, seems to induce rotation of

dx.doi.org/10.1021/ja304406c | J. Am. Chem. Soc. 2012, 134, 17932−17944

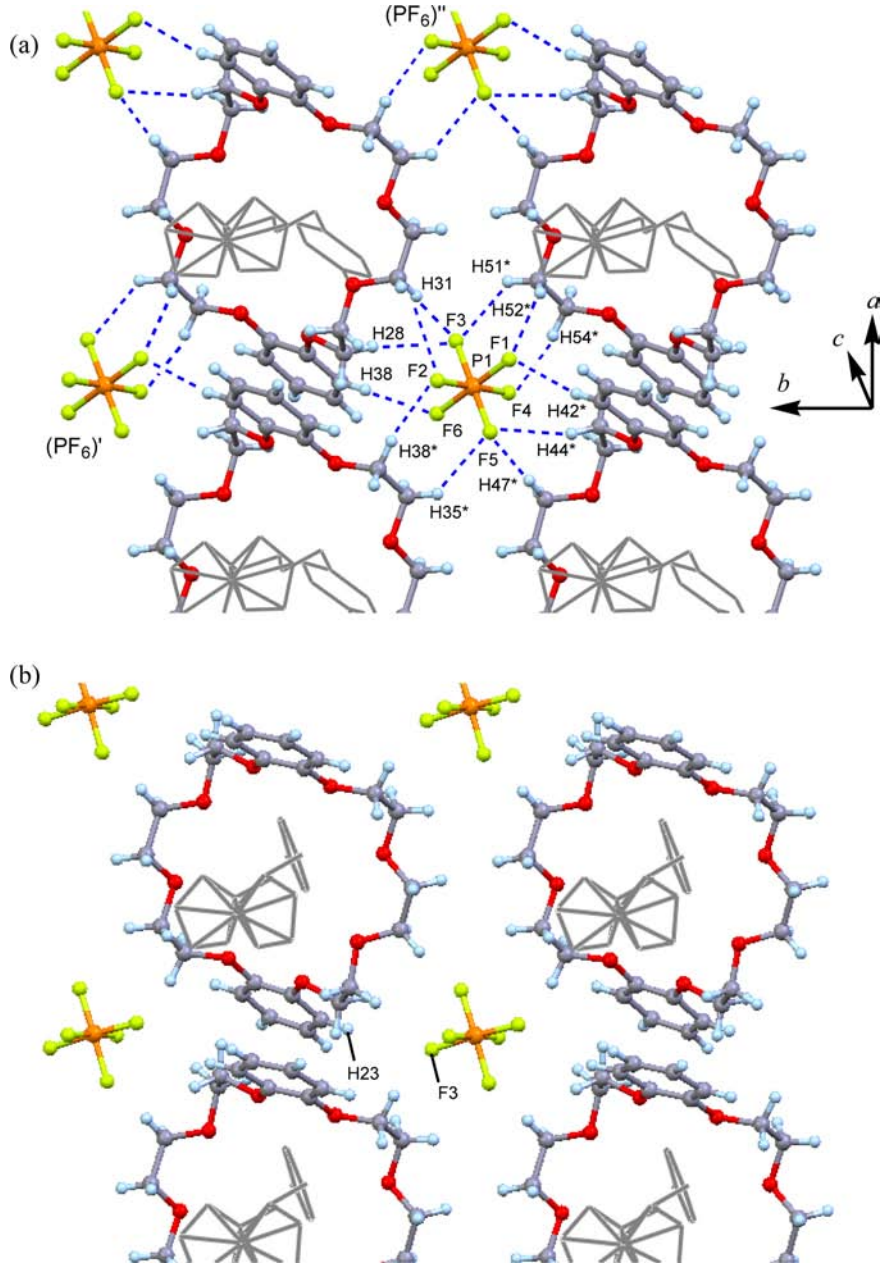

Figure 6. Geometries of intermolecular hydrogen bonds of **4** at (a) −150 °C and (b) 128 °C. A few hydrogen atoms were omitted for simplicity. Blue-dotted lines indicate geometric contacts between atoms.

the tolyl groups of the axle component **A** and **A**′; the two tolyl planes parallel to **B** and **B**′ are rotated upon the phase transition to adopt the conformation with C−H···π interaction with the catechol rings.

On the other hand, the pseudorotaxane **10** composed of the *N*-phenylmethyl group shows similar structure to that of **4** at 128 °C and **9** at −150 °C, forming C−H···π intrapseudorotaxane interaction and π−π interpseudorotaxane stacking (Figure 5d). DSC scan of **9** to lower temperature does not induce crystalline phase transition, suggesting that the observed crystal structure is not due to the phase transition below room temperature. The tolyl terminal group of **4** serves to stabilize its low temperature phase structure, but the phenyl group does not contribute to the stabilization of the structure with π−π stacking between the terminal phenyl and catechol planes. The *N*-phenylmethyl groups in the **10** are rather compact and flexible than the *N*-xylylmethyl groups having a methyl substituent, and prefer the structure with the interpseudorotaxane π−π stacking. The two phenyl groups of **10** fit well in a cavity surrounded by the catechol groups and form the C−H···π interaction rather than the π−π stacking interaction even at room temperature and below. X-ray crystal structure of **11** owing an ethyl terminal group on the axle molecule did not show significant intermolecular interaction, whereas the molecule showed π−π intermolecular interaction between aromatic rings of DB24C8 (Figure S4 in the Supporting Information). These results are regarded as the experimental proof to show importance of the terminal aryl group in the smooth crystalline phase transition of the pseudorotaxanes. In conclusion, the anisotropic shift of the PF_6^- anion of the pseudorotaxane plays a significant role to the crystalline phase transition of the pseudorotaxanes **4**-**7**, while the phase

dx.doi.org/10.1021/ja304406c | J. Am. Chem. Soc. 2012, 134, 17932−17944

transition is assisted also by DB24C8 with flexible structures and by the aryl groups.

Change in Crystal Dimensions and Optical Anisotropy. Measurement by a confocal laser microscope under a controlled temperature revealed a change in the shape of the crystal. Figure 7 shows reflection images of **4**, obtained by

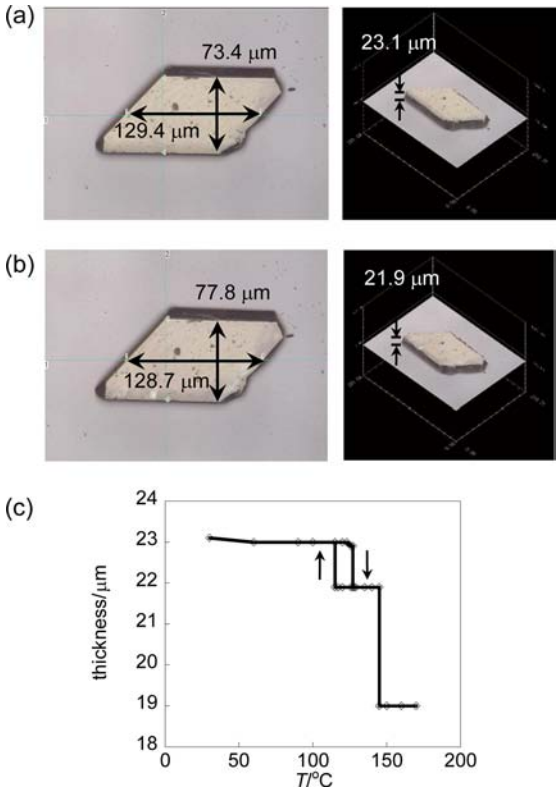

Figure 7. Reflection images of the **4** crystal obtained by laser microscopy at (a) 30 and (b) 128 °C. (c) Temperature dependence of thickness.

confocal laser microscopy. The pale-yellow crystals appear as thin trapezoidal plates having representative dimensions of 130 μm × 70 μm × 20 μm (**4**). At the transition temperature (128 °C), the horizontal, vertical, and thickness dimensions of the crystal changed by −0.5%, +6.0%, and −5.2%, respectively. The change in the crystal shape corresponds to the temperature-dependent change in the lattice parameters, observed by X-ray diffraction of the single crystals (Figures 3 and 7). The *a* axis remained unchanged at temperatures between 30 and 128 °C. In contrast, the *b* axis was 7.3% longer, the *c* axis was 4% shorter, and β was greater at 128 °C than at 30 °C. The crystal's dimensions are shown in Figure 3d along with the crystal axes and indexes. An approximate dynamic similarity was observed between the dimensions of the single crystal and those of the unit cell. These results arise from the movement of the aromatic group of the axle molecule, which rotates in the direction of the *b* axis to elongate the unit cell along this axis. In the vertical direction, the axle molecular pairs rotate by two molecules, the unit cell is pushed up and down along the *b* axis, and the crystal expands vertically. On the other hand, in the thickness direction, the free space between the two molecules in the unit cell is filled after the phase transition, the unit cell becomes thinner along the *c* axis, and the thickness of the crystal is decreased. Consequently, the motions on a molecular level can be related to change in the macroscopic crystal shape, which is induced by the rotation of the aromatic moiety of the axle molecules.

Single crystals of pseudorotaxane **4** have different structures at 30 and 128 °C owing to first-order thermal transitions, and this reversible structural change in a single crystal of the pseudorotaxane can be used to switch the anisotropy by controlling the temperature. This change in the crystal structure results from the rotation of the aromatic ring of the axle component, and the rotation of the molecules changes the anisotropy of the crystal. One of the most striking anisotropic properties of crystals is their optical anisotropy, which involves optical retardation and birefringence. Typically, the (001) face of the crystal plate exhibits an instantaneous switch in the interference color under a crossed polarizer microscope at the transition temperature. The color switches from green to orange when the crystal temperature is raised above the transition temperature at 128 °C, and the color returns to green when the crystal is cooled to below 116 °C. This color change occurs with a response time of less than 68 ms at a heating or cooling rate of 2 °C min^{-1} (see Supporting Information, Figure S5), and can be repeated more than 10 times. Below, we describe the details of the optical anisotropic switching of the pseudorotaxane crystal induced by dynamic motion of the axle molecule.

The angular dependence of the intensity of the transmitted light was observed by rotating the crossed-polarizer system and connecting the polarizing microscope to a monochromic charge-coupled device (CCD) detector, as shown in Figure 8. The highest transmittance appears at each 90° angle corresponding to a bright field that is in the lowest position to interact with the polarized light. The lowest transmittance appears at each 90° angle corresponding to the dark field and optical axis of the crystal, at which the polarized light interacts

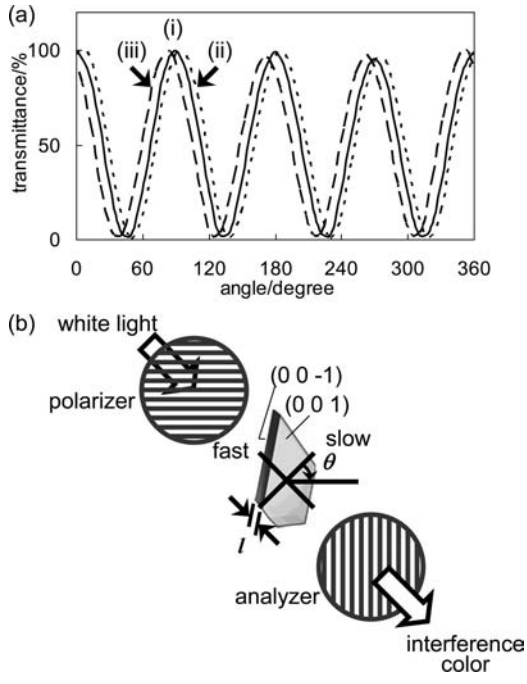

Figure 8. (a) Transmittance of **4** crystal (i) at 30 °C, (ii) from (001) face at 128 °C, and (iii) from (00 −1) face at 128 °C. (b) Optical system, where θ is the angle of the vibration plane of the crystal to that of the polarizer, and *l* is the thickness.

dx.doi.org/10.1021/ja304406c | J. Am. Chem. Soc. 2012, 134, 17932−17944

with the crystal most efficiently. The phase of the transmitted light of the single crystal **4** shifted to a higher angle of +12° on the (001) face at the first-order phase transition at 128 °C. Conversely, the optical axis and phase shifted to −12° on the (00 −1) face at 128 °C. According to X-ray diffraction analysis, the crystal was triclinic, which is optically anisotropic and biaxial. Conoscopic images of the crystal also showed an optically biaxial feature (see Supporting Information, Figure S6). However, optical slow and fast axes were observed as the effective optical axes which correspond to the angles at the lowest transmittance in Figure 8a.

Figure 9 shows the temperature dependence of the optical parameters θ (angle of the optical slow axis of the crystal to the

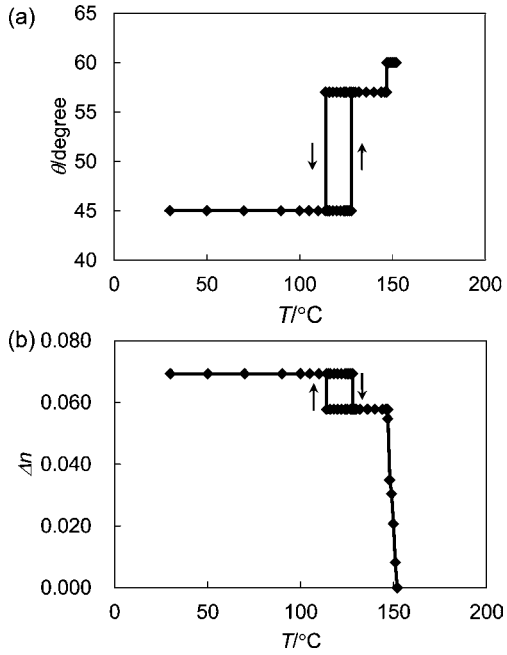

Figure 9. Temperature dependence of optical parameters of **4** crystal. (a) Angle of the vibration plane of the crystal to that of the polarizer. (b) Birefringence.

polarizer) and Δn (birefringence) of crystal **4** observed using a crossed polarizer microscope and a Berek compensator.[20−22] More accurate determinations of the Δn values for the crystal **4** than those of the previous our work[17] was conducted by the Berek compensator and taking an average Δn value of 10 crystals. Both parameters changed at the transition temperatures. On heating, θ increased from 45 to 57° on the (001) face of the crystal, and the crystal underwent axis rotation in the reverse direction on the (00 −1) face with the same degree of rotation from 45 to 33° at 128 °C. Corresponding changes were clearly observed in Δn. The Δn value of the crystal changed from 0.070 to 0.059, which corresponded to a decrease in the birefringence of 16% at 30 °C. Note that the original birefringence of the crystal was relatively large, as much as six times that of a quartz crystal. Further changes in θ and Δn were observed at 150 °C; however, the molecular structure was unclear because of the difficulty in single crystal X-ray diffraction analysis at higher temperatures.

The Δn values of crystals **4**−**9**, which contain various ratios of counteranions (PF_6^-:AsF_6^-) were also observed. In these measurements, more than 10 crystals containing each of the compositions were selected; the average values were plotted with error bars (see Figure 10). The lower experimental error for **4** is due to the high quality of single crystals of **4**. At 30 °C,

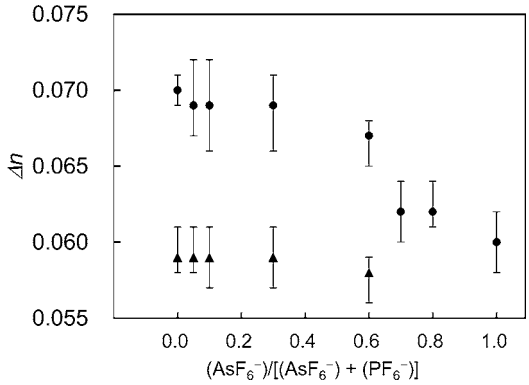

Figure 10. Plots of birefringence of crystals **4**−**9** with various ratios of counteranions PF_6^- and AsF_6^- at 30 °C (circles) and at the respective transition temperatures (triangles).

crystals of **4**−**7** exhibited similar Δn values ranging from 0.069 to 0.070 regardless of the anion composition ratio. All these Δn values were decreased to 0.059 at temperatures above the phase-transition temperatures. On the other hand, crystals of **8** (PF_6^-/AsF_6^- = 3:7) and **9** (AsF_6^- only) showed a lower Δn (0.062−0.060) than that of **4**−**9** at 30 °C. The Δn value of crystal **10** was also observed to be lower (0.055) at 30 °C. These results indicate that the conformation of the pseudorotaxanes, particularly the arrangement of the aromatic rings of the axle molecules, is dominated by birefringence rather than by other factors such as anion composition and density. However, the crystals with higher AsF_6^- compositions showed less reversible phase transitions, and the crystals tended to crack when they were returned to a lower-temperature phase.

The interference color can generally be observed in optically anisotropic crystals through crossed polarizers. The color originates from the two vibrational planes of the crystal, which produce two optical wave components with differing phase velocities and orthogonal oscillating directions for the incident light. When linearly polarized white light enters the crystal, the total optical field at the crystal exit varies in strength and polarization depending on the wavelength. Therefore, the crystal appears colored through the analyzer. The degree of variation in the strength and polarization is controlled by varying the angle of the vibrational plane of the crystal to that of the polarizer, θ, and the retardation, Ψ ($\Psi \propto \Delta n \cdot l$). The thickness of the **4** crystal changed by 5%, which is relatively small compared to the variation in θ (12°) and Δn (16%). Consequently, the interference color change is mainly due to the variation in θ and Δn.

The relationship between changes in the optical parameters of the crystal and those in the molecular structure are described hereafter. Figure 11 shows the projection of the molecules and the (001) face of crystals **4**, **9**, and **10**. All of the aryl planes of the axle and cyclic molecules in **4** are parallel at 30 °C, whereas the aryl planes of the axle molecules in **4** are tilted from the aryl planes of DB24C8 by 37° at 128 °C. One would expect greater anisotropy and birefringence for the crystal at 30 °C than at 128 °C. Measurement of the rotation of the crossed polarized plates (Figure 8b) revealed that at 30 °C, the face of the phenyl rings of the rotaxanes lay almost parallel to the optical fast axis of the crystal and perpendicular to its slow axis. Consequently, greater

dx.doi.org/10.1021/ja304406c | J. Am. Chem. Soc. 2012, 134, 17932−17944

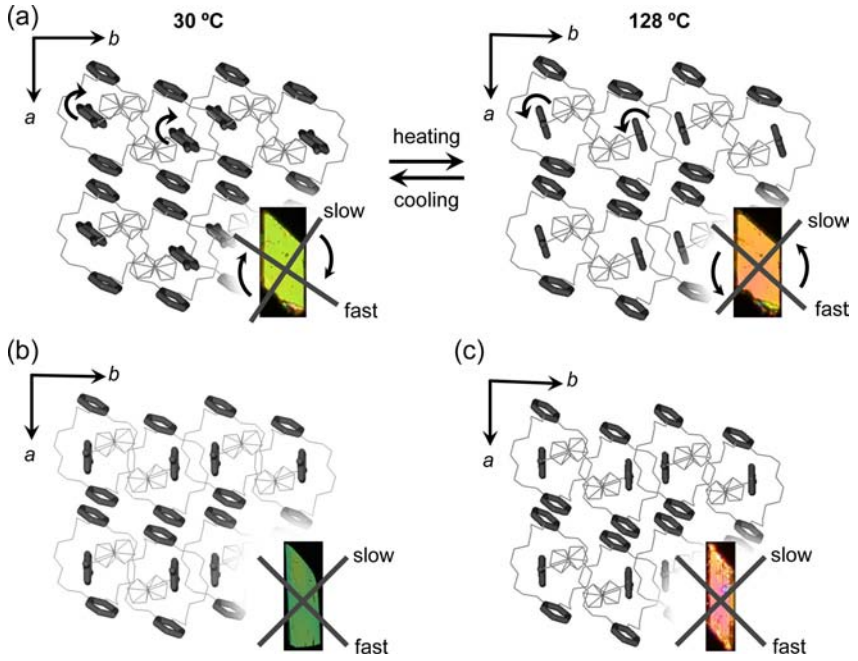

Figure 11. Molecular structures of pseudorotaxane (a) **4**, (b) **9**, and (c) **10** projected from (001) face. Optical slow and fast axes are superimposed on the crystal images.

polarizability or electrostatic interaction exists in the slow-axis direction than that in the fast-axis direction. The rotation of the *p*-tolyl planes of the axle molecules due to the crystalline-phase transition (heating) induces rotation of the optical axes of the crystal in the same direction. The direction of this rotation was opposite when it was observed from the back face, thereby indicating that the direction of optical-axis rotation is controlled by the rotation of the *p*-tolyl planes of the axle molecules. Birefringence is also reduced effectively by rotation of the aromatic planes owing to the disordered alignment of the aromatic rings at higher temperatures.

The optical axes of **9** and **10** appeared in a similar position to those of the high-temperature phase of **4** owing to their similar alignments. Birefringences of **9** (Δn = 0.060) and **10** (Δn = 0.055) at 30 °C were lower than that of the low-temperature phase of **4** (Δn = 0.070) owing to the disordered alignment of the aromatic rings of **9** and **10**.

CONCLUSION

We have discovered a first-order thermal transition of the pseudorotaxane crystal that corresponds to partial structural changes of the axle molecules in the crystal. The reversible phase transition causes rotation of the aryl terminal group of the axle molecule. The bulky and metal-containing ferrocenyl group at the other end does not participate in major motion of the rotaxane, and serves to keep the conformation of the axle molecule, except for the aryl terminal group, during the crystalline phase transition. The pseudorotaxanes, having aryl groups at the both ends,[23] did not undergo such reversible phase transition. In the crystals, the composition ratios of PF_6^- and AsF_6^- are essential to determine the inter- and intra-pseudorotaxane interactions as well as the phase-transition temperatures. The reversible rotary motion of the end group of the interlocked axle molecule of the pseudorotaxane can change the anisotropy of the crystal, which involves the crystal shape and the optical anisotropy. The highly ordered molecular alignment within the crystal enables a change in the crystal's optical anisotropy. Changing the substituents and components of the pseudorotaxanes can result in a desired change in the crystal's birefringence. The birefringence and arrangement of the axle molecules should be key parameters for light-wave control of the optically anisotropic crystals. The pseudorotaxane crystals can control these parameters dynamically through the collective motion of the pseudorotaxane units.

EXPERIMENTAL SECTION

General Methods. Synthesis and crystallization of **4**–**9** were carried out according to the literature method,[9,17] and compound **10** was prepared by analogous method. DB24C8 was purchased from Tokyo Kasei Kogyo Co., Ltd. ^{1}H and ^{13}C{^{1}H} NMR spectra were recorded on JEOL EX-400 or Varian Mercury 300 spectrometers. The chemical shifts were referenced with respect to $CHCl_3$ (δ 7.24), CD_2HCN (δ 1.93) for ^{1}H and $CDCl_3$ (δ 77.0), CD_3CN (δ 1.30) for ^{13}C as internal standards. IR absorption spectra were recorded on Shimadzu FT/IR-8100 spectrometers. Elemental analyses were carried out with a Yanaco MT-5 CHN autorecorder. ICP (inductively coupled plasma) analysis was conducted by ICPS-8000 (SHIMADZU Corporation). DSC was recorded by Seiko instrument DSC6200S. Thermogravimetric analysis (TGA) was recorded on Seiko TG/DTA6200R. Crystal data for structure analyses, cell determination, and face indices of the crystal were collected by a diffractometer (RIGAKU AFC-8) with CCD detector (Saturn 70) using Mo Kα radiation. Temperature was controlled on X-ray diffraction measurements by a nitrogen gas stream heating technique using a RIGAKU high temperature heating devise.

Preparation of $1^+AsF_6^-$. To a suspension of 1^+Cl^- (724 mg, 2.0 mmol) in acetone (15 mL) was added $KAsF_6$ (2.31 g, 10.1 mmol) in acetone (15 mL), and the mixture was stirred for 2 h at room temperature. The precipitate was removed by filtration. Evaporation of the filtrate gave crude product which was washed with water and diethylether to yield $1^+AsF_6^-$ as a yellow solid (582 mg, 1.14 mmol, 56%). Anal. Calcd. for $C_{19}H_{22}NF_6FeAs$: C, 44.82; H, 4.36; N, 2.75. Found: C, 44.44; H, 4.37; N, 2.68. ^{1}H NMR spectrum (300 MHz, CD_3CN, rt): δ 2.34 (s, 3H, CH_3), 4.04 (brs, 2H, CH_2), 4.06 (brs, 2H, CH_2), 4.21 (s, 5H, C_5H_5), 4.27 (m, 2H, C_5H_4), 4.37 (m, 2H, C_5H_4), 7.25 (d, 2H, C_6H_4, J = 8.4 Hz), 7.30 (d, 2H, C_6H_4, J = 8.1 Hz). ^{13}C{^{1}H} NMR spectrum (75.5 MHz, CD_3CN, r. t.): δ 21.3 (CH_3),

dx.doi.org/10.1021/ja304406c | J. Am. Chem. Soc. 2012, 134, 17932–17944

48.7 (CH_2), 51.6 (CH_2), 70.0 (C_5H_5), 70.5 (C_5H_4), 71.5 (C_5H_4), 76.4 (C_5H_4), 128.5 (C_6H_4), 130.6 (C_6H_4), 131.0 (C_6H_4), 140.8 (C_6H_4). IR spectrum (KBr): ν = 3250 (N−H), 3225 (N−H), 675 (As−F) cm^{-1}. Five percent weight loss by thermogravimetry: 235 °C.

Isolation of [1(DB24C8)]$^+$AsF$_6^-$ (9). Yellow crystals of pseudorotaxane [**1**(DB24C8)]$^+$$AsF_6^-$ was obtained by recrystallization from a $CHCl_3$/hexane solution of **1**$^+$$AsF_6^-$/DB24C8 (**1**$^+$$AsF_6^-$/DB24C8 = 51 mg/45 mg). [**1**(DB24C8)]$^+$$AsF_6^-$ was obtained in 82% (0.082 mmol). Anal. Calcd. for $C_{43}H_{54}NF_6FeAsO_8$: C, 53.43; H, 5.73; N, 1.45. Found: C, 53.40; H, 5.67; N, 1.45. IR spectrum (KBr): ν = 3067 (N−H), 3171 (N−H), 700 (As−F) cm^{-1}. Five percent weight loss by thermogravimetry: temperature 260 °C.

Preparation of 2$^+$PF$_6^-$. To a suspension of **2**$^+$$Cl^-$ (3.4 g, 10 mmol) in acetone (100 mL) was added NH_4PF_6 (8.5 g) in acetone (100 mL), and the mixture was stirred for 2 h at room temperature. The precipitate was removed by filtration. Evaporation of the filtrate gave crude product which was washed with CH_2Cl_2, Et_2O and water and dried under reduced pressure to yield **2**$^+$$PF_6^-$ as an orange solid (1.80, 4.0 mmol, 40%). Anal. Calcd. for $C_{18}H_{20}F_6FeNP$: C, 47.92; H, 4.47; N, 3.10. Found: C, 47.53; H, 4.35; N, 2.97. ^{1}H NMR (300 MHz, CD_3CN, r. t.): δ 4.06 (s, 2H, CH_2), 4.11 (s, 2H, CH_2), 4.21 (s, 5H, C_5H_5), 4.28 (m, 2H, C_5H_4), 4.38 (m, 2H, C_5H_4), 7.40−7.46 (5H, Ph). ^{13}C{^{1}H} NMR (75.5 MHz, CD_3CN, r. t.): δ 48.4 (CH_2), 51.5 (CH_2), 69.9 (C_5H_5), 70.5 (C_5H_4), 71.4 (C_5H_4), 76.6 (C_5H_4-ipso), 130.0 (Ph), 130.5 (Ph), 130.9 (Ph), 131.8 (Ph-ipso). IR (KBr disk): ν = 3262 (N−H), 3236 (N−H), 843 (P−F), 559 (P−F) cm^{-1}.

Isolation of [2(DB24C8)]$^+$PF$_6^-$ (10). Yellow crystals of pseudorotaxane [**2**(DB24C8)]$^+$$PF_6^-$ was obtained by recrystallization from a CH_2Cl_2/Et_2O (4 mL/7 mL) solution of **2**$^+$$PF_6^-$/DB24C8 (**2**$^+$$PF_6^-$/DB24C8 = 59 mg/47 mg). 71% yield (0.071 mmol). Anal. Calcd. for $C_{42}H_{52}NO_8F_6FeP$: C, 56.07; H, 5.83; N, 1.56. Found: C, 55.90; H, 5.72; N, 1.50. IR spectrum (KBr): ν = 3156 (N−H), 3065 (N−H), 841 (P−F), 558 (P−F) cm^{-1}. 5% weight loss by thermogravimetry: 227 °C.

Preparation of FcCH$_2$NHEt (3). To a solution of ferrocenecarboxyaldehyde (2.13 g, 10 mmol) in MeOH (50 mL) was added $EtNH_2$ (2.0 M methanol solution, 6.0 mL, 12 mmol) at room temperature. The mixture was stirred at 50 °C for 17 h. Evaporation of the solution to dryness produced FcCH═NEt as brown oil (2.25 g, 0.3 mmol, 93%) [^{1}H NMR (300 MHz, $CDCl_3$, rt): δ 1.23 (t, 3H, Me, J = 7 Hz), 3.46 (q, 2H, CH_2, J = 7 Hz), 4.16 (s, 5H, C_5H_5), 4.35 (m, 2H, C_5H_4), 4.64 (m, 2H, C_5H_4), 8.10 (s, 1H, N = CH). ^{13}C{^{1}H} NMR (100 MHz, $CDCl_3$, rt): δ 16.4 (Me), 55.8 (CH_2), 68.3 (C_5H_4), 69.0 (C_5H_5), 70.2 (C_5H_4), 80.5 (C_5H_4), 160.2 (C═N)]. The above product (2.1 g, 8.7 mmol) was dissolved in MeOH (40 mL) at room temperature. $NaBH_4$ (800 mg, 21 mmol) was added to the solution and the mixture was stirred for 12 h at room temperature. The reaction mixture was added with 1 M HCl (90 mL) to form brown suspension. One M KOH (100 mL) was added to the solution to cause the separation of orange solid, which was partitioned between water and hexane. Organic extract was washed with water (3 times), dried over $MgSO_4$, filtered, and concentrated under reduced pressure to give $FcCH_2NHEt$ as a brown oil (1.91 g, 7.9 mmol, 91%). ^{1}H NMR (300 MHz, $CDCl_3$, rt): δ 1.12 (t, 3H, Me, J = 7 Hz), 2.68 (q, 2H, MeCH_2, J = 7 Hz), 3.53 (s, 2H, $FcCH_2$), 4.06−4.15 (3H, C_5H_4, NH), 4.11 (s, 5H, C_5H_5), 4.19 (m, 2H, C_5H_4). ^{13}C{^{1}H} NMR (100 MHz, $CDCl_3$, rt): δ 15.2 (Me), 43.7 (NCH_2), 48.8 (NCH_2), 67.7 (C_5H_4), 68.3 (C_5H_5), 68.4 (C_5H_4), 87.0 (C_5H_4). IR spectrum (neat): ν = 3315 (N−H) cm^{-1}.

Preparation of 3$^+$PF$_6^-$. To a solution of $FcCH_2NHEt$ (1.90 g, 7.8 mmol) in MeOH (10 mL) was added 1 M HCl (7.8 mL) at room temperature to cause separation of yellow solid. The obtained suspension was poured into an acetone solution (80 mL) of NH_4PF_6 (4.0 g, 25 mmol) to form brown solution. Addition of acetone (200 mL) to the solution cause the separation of yellow solid which was collected by filtration and dried in vacuo to yield [$FcCH_2NH_2Et$]$^+$$PF_6^-$ (1.74 g, 4.5 mmol, 58%). Anal. Calcd. for $C_{13}H_{18}NF_6FeP$: C, 40.13; H, 4.66; N, 3.60. Found: C, 40.14; H, 4.66; N, 3.60. ^{1}H NMR spectrum (400 MHz, acetone-d_6, rt): δ 1.27 (t, 3H, Me, J = 7 Hz), 3.22 (q, 2H, MeCH_2, J = 7 Hz), 4.11 (s, 5H, C_5H_5), 4.17 (m, 2H), 4.26 (m, 2H), 4.35 (m, 2H). ^{13}C{^{1}H} NMR (100 MHz, acetone-d_6, rt): δ 11.5 (Me), 43.7 (NCH_2), 48.5 (NCH_2), 69.8 (C_5H_5), 70.4 (C_5H_4), 71.2 (C_5H_4), 77.2 (C_5H_4). IR spectrum (KBr): ν = 3271 (N−H), 3245 (N−H), 833 (P−F), 558 (P−F) cm^{-1}. Five percent weight loss by thermogravimetry: 196 °C.

Isolation of [3(DB24C8)]$^+$PF$_6^-$ (11). Yellow crystals of pseudorotaxane [$FcCH_2NH_2Et$(DB24C8)]$^+$$PF_6^-$ were obtained by vapor diffusion of Et_2O into a solution of [$FcCH_2NH_2Et$]$^+$$PF_6^-$ (**3**$^+$$PF_6^-$) (47 mg, 0.12 mmol) and DB24C8 (47 mg, 0.11 mmol) in CH_2Cl_2 (1.0 mL). **11** was obtained in 70% (70 mg, 0.084 mmol). Anal. Calcd. for $C_{37}H_{50}NF_6FeO_8P(H_2O)_{0.5}$: C, 52.49; H, 6.07; N, 1.65. Found: C, 52.33; H, 5.86; N, 1.73. IR spectrum (KBr): ν = 3185 (N−H), 3065 (N−H), 840 (P−F), 557 (P−F) cm^{-1}. Five percent weight loss by thermogravimetry: 234 °C.

Typical Procedure for the Preparation of [1(DB24C8)$^+$](PF$_6^-$)$_{1-x}$(AsF$_6^-$)$_x$ (x = 0.05, 0.1, 0.3, 0.7). Yellow crystals of pseudorotaxane [**1**(DB24C8)]$^+$$(PF_6^-)_{0.44}(AsF_6^-)_{0.53}$ were obtained by recrystallization from a $CHCl_3$/acetone/hexane solution of **1**$^+$$PF_6^-$/**1**$^+$$AsF_6^-$/DB24C8 (0.050 mmol/0.050 mmol/0.10 mmol) at room temperature. [**1**(DB24C8)]$^+$$(PF_6^-)_{0.44}(AsF_6^-)_{0.53}$ was obtained in 47%. The content of P and As was analyzed by elemental analysis, X-ray crystallography and ICP (inductively coupled plasma) analysis.

Other pseudorotaxanes [**1**(DB24C8)]$^+$$(PF_6^-)_{1-x}(AsF_6^-)_x$ (x = 0.05, 0.1, 0.3, 0.7) was prepared similarly by recrystallization from a $CHCl_3$/acetone/hexane solution. The contents of P and As (Figure 2) in obtained pseudorotaxanes were estimated to be same to the initial concentration of **1**$^+$$PF_6^-$ and **1**$^+$$AsF_6^-$. The phase transition temperature of these pseudorotaxanes, [**1**(DB24C8)]$^+$$(PF_6^-)_{1-x}(AsF_6^-)_x$ (x = 0.05, 0.1, 0.3, 0.5, 0.7), in the solid state was analyzed by DSC measurement.

Crystal Structure Analysis. Crystals of **4**, **8**, **9**, **10**, and **11** suitable for X-ray diffraction study were obtained by recrystallization from CH_2Cl_2/Et_2O, CH_2Cl_2/acetone/hexane, $CHCl_3$/hexane, CH_2Cl_2/Et_2O, and CH_2Cl_2/Et_2O, respectively, and mounted on glass capillary tubes. The data were collected to a maximum 2θ value of 55.0°. A total of 720 oscillation images were collected. A sweep of data was done using ω scans from −110.0 to 70.0° in 0.5° step, at χ = 45.0° and ϕ = 0.0°. The detector swing angle was −20.42°. A second sweep was performed using ω scans from −110.0 to 70.0° in 0.5° step, at χ = 45.0° and ϕ = 90.0°. The crystal-to-detector distance was 44.84 mm. Readout was performed in the 0.070 mm pixel mode. Calculations were carried out by using a program package Crystal Structure for Windows. The structure was solved by direct methods and expanded using Fourier techniques. A full-matrix least-squares refinement was used for the non-hydrogen atoms with anisotropic thermal parameters. Crystal data and detailed results of refinement are summarized in Table S1 in the Supporting Information.

Crystallographic data have been deposited at the CCDC, 12 Union Road, Cambridge CB21EZ, UK and copies can be obtained on request, free of charge, by quoting the publication citation and the deposition numbers, 235382, 257706, 257707, and 903277 - 903280.

Optical Measurements. The thermo-optical properties of the crystal were observed in polarizing microscope (Olympus BX51-P) with temperature control by the combination of central processor and hot stage (LINKAM TMS92 and THMS600). The monochromic light was generated by using color filter (Olympus 43IF550-W45). The intensity of the transmitted light was monitored by a monochromic CCD camera (Hamamatsu Photonics C5948) and a video image enhancement system (DVS-20) connecting to the polarizing microscope (Nikon ECLIPSE E600POL). The optical fast and slow axes were determined by the direction of the polarizer and analyzer pair at the extinction (0°) and diagonal position (45°) using a 1/4λ plate (Olympus U-TP137). In obtaining the birefringences ($\Delta n = n_e - n_o$), the slow and the fast axes, which respectively indicate directions of the vibration exhibiting large refractive index and the small index, were also determined using a wavelength of 550 nm. The interference color were converted into the optical anisotropic parameters of the optical retardations using the Michel Lévy chart (Nikon interference color chart), a quartz wedge (Olympus U-CWE2), Sénarmont compensator (Olympus U-CSE), and Berek compensator (Olympus U-CBE) under observations with white and monochromatic light at 550 nm. The

thickness and shape of the crystals was observed by confocal laser microscope (KEYENCE VK-9510) with temperature control by using the combination of central processor and hot stage (Mettler FP90 and FP82HT). The thickness of the crystals was also estimated using the polarizing microscope (Olympus BX51-P). Δn was obtained from the optical retardation and thickness of the crystal.

■ ASSOCIATED CONTENT

Supporting Information

Crystal data, IR spectra, DSC charts, crystal structure of **11**, and conoscopic images. This material is available free of charge via the Internet at http://pubs.acs.org.

■ AUTHOR INFORMATION

Corresponding Author

mhorie@mx.nthu.edu.tw

Notes

The authors declare no competing financial interest.

■ ACKNOWLEDGMENTS

We are grateful to Dr. A. M. Spring of University of Manchester for enlightening discussion. We thank the Center for Advanced Materials Analysis, Technical Department, Tokyo Institute of Technology for elemental analysis and ICP analysis. This work was financially supported by National Science Council of Taiwan, Ministry of Education, Culture, Sports, Science, and Technology, Japan, and the Mazda foundation.

■ REFERENCES

(1) (a) Coskun, A.; Banaszak, M.; Astumian, R. D.; Stoddart, J. F.; Grzybowski, B. A. *Chem. Soc. Rev.* **2012**, *41*, 19−30. (b) Balzani, V.; Credi, A.; Venturi, M. *Molecular Devices and Machines*, 2nd ed.; Wiley-VCH: Weinheim, 2008. (c) Fang, L.; Olson, M. A.; Benitez, D.; Tkatchouk, E.; Goddard, W. A.; Stoddart, J. F. *Chem. Soc. Rev.* **2010**, *39*, 17−29. (d) Stoddart, J. F. *Chem. Soc. Rev.* **2009**, *38*, 1802−1820. (e) Badjic, J. D.; Nelson, A.; Cantrill, S. J.; Turnbull, W. B.; Stoddart, J. F. *Acc. Chem. Res.* **2005**, *38*, 723−732. (f) Balzani, V.; Credi, A.; Raymo, F. M.; Stoddart, J. F. *Angew. Chem., Int. Ed.* **2000**, *39*, 3349−3391.

(2) (a) Aida, T.; Meijer, E. W.; Stupp, S. I. *Science* **2012**, *335*, 813−817. (b) Tanaka, H.; Ikeda, T.; Takeuchi, M.; Sada, K.; Shinkai, S.; Kawai, T. *ACS Nano* **2011**, *5*, 9575−9582. (c) Ogi, S.; Ikeda, T.; Wakabayashi, R.; Shinkai, S.; Takeuchi, M. *Chem.—Eur. J.* **2010**, *16*, 8285−8290. (d) Takeuchi, M.; Ikeda, M.; Sugasaki, A.; Shinkai, S. *Acc. Chem. Res.* **2001**, *34*, 865−873. (e) Barbara, P. F. *Acc. Chem. Res.* **2001**, *34*, 409−522. (f) Stupp, S. I. *Chem. Rev.* **2005**, *105*, 1023−1562. (g) Kinbara, K.; Aida, T. *Chem. Rev.* **2005**, *105*, 1377−1400.

(3) (a) Beves, J. E.; Blight, B. A.; Campbell, C. J.; Leigh, D. A.; McBurney, R. T. *Angew. Chem., Int. Ed.* **2011**, *50*, 9260−9327. (b) von Delius, M.; Leigh, D. A. *Chem. Soc. Rev.* **2011**, *40*, 3656−3676. (c) Kay, E. R.; Leigh, D. A.; Zerbetto, F. *Angew. Chem., Int. Ed.* **2007**, *46*, 72−191. (d) Kottas, G. S.; Clarke, L. I.; Horinek, D.; Michl, J. *Chem. Rev.* **2005**, *105*, 1281−1376.

(4) (a) McDowell, J. J.; Zacharia, N. S.; Puzzo, D.; Manners, I.; Ozin, G. A. *J. Am. Chem. Soc.* **2010**, *132*, 3236−3237. (b) Puzzo, D. P.; Arsenault, A. C.; Manners, I.; Ozin, G. A. *Angew. Chem., Int. Ed.* **2009**, *48*, 943−947. (c) Ozin, G. A.; Manners, I.; Fournier-Bidoz, S.; Arsenault, A. *Adv. Mater.* **2005**, *17*, 3011−3018.

(5) (a) Eelkema, R.; Pollard, M. M.; Vicario, J.; Katsonis, N.; Ramon, B. S.; Bastiaansen, C. W. M.; Broer, D. J.; Feringa, B. L. *Nature* **2006**, *440*, 163−163. (b) Kudernac, T.; Ruangsupapichat, N.; Parschau, M.; Macia, B.; Katsonis, N.; Harutyunyan, S. R.; Ernst, K. H.; Feringa, B. L. *Nature* **2011**, *479*, 208−211. (c) Wang, J. B.; Feringa, B. L. *Science* **2011**, *331*, 1429−1432. (d) Michl, J.; Sykes, E. C. H. *ACS Nano* **2009**, *3*, 1042−1048.

(6) (a) Anelli, P. L.; Spencer, N.; Stoddart, J. F. *J. Am. Chem. Soc.* **1991**, *113*, 5131−5133. (b) Bissell, R. A.; Córdova, E.; Kaifer, A. E.; Stoddart, J. F. *Nature* **1994**, *369*, 133−137. (c) Badjic, J. D.; Balzani, V.; Credi, A.; Silvi, S.; Stoddart, J. F. *Science* **2004**, *303*, 1845−1849. (d) Balzani, V.; Clemente-Leon, M.; Credi, A.; Ferrer, B.; Venturi, M.; Flood, A. H.; Stoddart, J. F. *Proc. Natl. Acad. Sci. U.S.A.* **2006**, *103*, 1178−1183. (e) Saha, S.; Stoddart, J. F. *Chem. Soc. Rev.* **2007**, *36*, 77−92. (f) Li, H.; Fahrenbach, A. C.; Coskun, A.; Zhu, Z. X.; Barin, G.; Zhao, Y. L.; Botros, Y. Y.; Sauvage, J. P.; Stoddart, J. F. *Angew. Chem., Int. Ed.* **2011**, *50*, 6782−6788.

(7) (a) Brouwer, A. M.; Frochot, C.; Gatti, F. G.; Leigh, D. A.; Mottier, L.; Paolucci, F.; Roffia, S.; Wurpel, G. W. H. *Science* **2001**, *291*, 2124−2128. (b) Alvarez-Perez, M.; Goldup, S. M.; Leigh, D. A.; Slawin, A. Z. *J. Am. Chem. Soc.* **2008**, *130*, 1836−1838. (c) Carlone, A.; Goldup, S. M.; Lebrasseur, N.; Leigh, D. A.; Wilson, A. *J. Am. Chem. Soc.* **2012**, *134*, 8321−8323. (d) Blanco, V.; Carlone, A.; Hanni, K. D.; Leigh, D. A.; Lewandowski, B. *Angew. Chem., Int. Ed.* **2012**, *51*, 5166−5169. (e) Panman, M. R.; Bodis, P.; Shaw, D. J.; Bakker, B. H.; Newton, A. C.; Kay, E. R.; Leigh, D. A.; Buma, W. J.; Brouwer, A. M.; Woutersen, S. *Phys. Chem. Chem. Phys.* **2012**, *14*, 1865−1875.

(8) (a) Durola, F.; Sauvage, J. P.; Wenger, O. S. *Coord. Chem. Rev.* **2010**, *254*, 1748−1759. (b) Durot, S.; Reviriego, F.; Sauvage, J. P. *Dalton Trans.* **2010**, *39*, 10557−10570. (c) Joosten, A.; Trolez, Y.; Collin, J. P.; Heitz, V.; Sauvage, J. P. *J. Am. Chem. Soc.* **2012**, *134*, 1802−1809. (d) Collin, J.-P.; Heitz, V.; Sauvage, J.-P. *Top. Curr. Chem.* **2005**, *262*, 29−62.

(9) (a) Horie, M.; Suzaki, Y.; Osakada, K. *J. Am. Chem. Soc.* **2004**, *126*, 3684−3685. (b) Horie, M.; Suzaki, Y.; Osakada, K. *Inorg. Chem.* **2005**, *44*, 5844−5853. (c) Suzaki, Y.; Taira, T.; Osakada, K.; Horie, M. *Dalton Trans.* **2008**, *36*, 4823−4833.

(10) (a) Juluri, B. K.; Kumar, A. S.; Liu, Y.; Ye, T.; Yang, Y. W.; Flood, A. H.; Fang, L.; Stoddart, J. F.; Weiss, P. S.; Huang, T. J. *ACS Nano* **2009**, *3*, 291−300. (b) Liu, Y.; Flood, A. H.; Bonvallet, P. A.; Vignon, S. A.; Northrop, B. H.; Tseng, H.-R.; Jeppesen, J. O.; Huang, T. J.; Brough, B.; Baller, M.; Magonov, S.; Solares, S. D.; Goddard, W. A.; Ho, C.-M.; Stoddart, J. F. *J. Am. Chem. Soc.* **2005**, *127*, 9745−9759.

(11) (a) Green, J. E.; Choi, J. W.; Boukai, A.; Bunimovich, Y.; Johnston-Halperin, E.; DeIonno, E.; Luo, Y.; Sheriff, B. A.; Xu, K.; Shin, Y. S.; Tseng, H.-R.; Stoddart, J. F.; Heath, J. R. *Nature* **2007**, *445*, 414−417. (b) Zhang, W. Y.; DeIonno, E.; Dichtel, W. R.; Fang, L.; Trabolsi, A.; Olsen, J. C.; Benitez, D.; Heath, J. R.; Stoddart, J. F. *J. Mater. Chem.* **2011**, *21*, 1487−1495.

(12) Berna, J.; Leigh, D. A.; Lubomska, M.; Mendoza, S. M.; Perez, E. M.; Rudolf, P.; Teobaldi, G.; Zerbetto, F. *Nat. Mater.* **2005**, *4*, 704−710.

(13) (a) MacGillivray, L. R.; Papaefstathiou, G. S.; Friscic, T.; Hamilton, T. D.; Bucar, D. −K.; Chu, Q.; Varshney, D. B.; Georgiev, I. G. *Acc. Chem. Res.* **2008**, *41*, 280−291. (b) Sokolov, A. N.; Swenson, D. C.; MacGillivray, L. R. *Proc. Natl. Acad. Sci. U.S.A.* **2008**, *105*, 1794−1797. (c) Kobr, L.; Zhao, K.; Shen, Y. Q.; Comotti, A.; Bracco, S.; Shoemaker, R. K.; Sozzani, P.; Clark, N. A.; Price, J. C.; Rogers, C. T.; Michl, J. *J. Am. Chem. Soc.* **2012**, *134*, 10122−10131. (d) Setaka, W.; Yamaguchi, K. *Proc. Natl. Acad. Sci. U.S.A.* **2012**, *109*, 9271−9275.

(14) (a) Li, Q. W.; Zhang, W. Y.; Miljanic, O. S.; Sue, C. H.; Zhao, Y. L.; Liu, L. H.; Knobler, C. B.; Stoddart, J. F.; Yaghi, O. M. *Science* **2009**, *325*, 855−859. (b) Vukotic, V. N.; Harris, K. J.; Zhu, K. L.; Schurko, R. W.; Loeb, S. J. *Nat. Chem.* **2012**, *4*, 456−460. (c) Coskun, A.; Hmadeh, M.; Barin, G.; Gandara, F.; Li, Q. W.; Choi, E.; Strutt, N. L.; Cordes, D. B.; Slawin, A. M. Z.; Stoddart, J. F.; Sauvage, J. P.; Yaghi, O. M. *Angew. Chem., Int. Ed.* **2012**, *51*, 2160−2163. (d) Deng, H. X.; Olson, M. A.; Stoddart, J. F.; Yaghi, O. M. *Nat. Chem.* **2010**, *2*, 439−443.

(15) (a) Vogelsberg, C. S.; Garcia-Garibay, M. A. *Chem. Soc. Rev.* **2012**, *41*, 1892−1910. (b) Garcia-Garibay, M. A. *Proc. Natl. Acad. Sci. U.S.A.* **2005**, *102*, 10771−10776. (c) Khuong, T.-A. V.; Nunez, J. E.; Godinez, C. E.; Garcia-Garibay, M. A. *Acc. Chem. Res.* **2006**, *39*, 413−422. (d) Garcia-Garibay, M. A. *Angew. Chem., Int. Ed.* **2007**, *46*, 8945−8947. (e) Rodriguez-Molina, B.; Farfan, N.; Romero, M.; Mendez-

Stivalet, J. M.; Santillan, R.; Garcia-Garibay, M. A. *J. Am. Chem. Soc.* **2011**, *133*, 7280−7283.
(16) (a) Akutagawa, T.; Sato, D; Koshinaka, H.; Aonuma, M.; Noro, S. I.; Takeda, S.; Nakamura, T. *Inorg. Chem.* **2008**, *47*, 5951−5962. (b) Akutagawa, T.; Koshinaka, H.; Sato, D.; Takeda, S.; Noro, S. I.; Takahashi, H.; Kumai, R.; Tokura, Y.; Nakamura, T. *Nat. Mater.* **2009**, *8*, 342−347.
(17) Horie, M.; Sassa, T.; Hashizume, D.; Suzaki, Y.; Osakada, K.; Wada, T. *Angew. Chem., Int. Ed.* **2007**, *46*, 4983−4986.
(18) (a) Wiebcke, M.; Mootz, D. *Z. Kristallogr.* **1988**, *183*, 1−13. (b) Cook, D. *Chem. Ind.* **1963**, 607−8.
(19) Tsuzuki, S.; Honda, K.; Uchimaru, T.; Mikami, M.; Tanabe, K. *J. Am. Chem. Soc.* **2002**, *124*, 104−112.
(20) Hecht, E. *Optics*; 4th ed.; Addison Wesley, San Francisco, CA, USA, 2001.
(21) Demus, D.; Goodby, J.; Gray, G. W.; Spiess, H.-W.; Vill, V. *Handbook of Liquid Crystals*; Wiley-VCH: Weinheim, 1998; Vol. 2*A*.
(22) Sigman, M. B.; Korgel, B. A. *J. Am. Chem. Soc.* **2005**, *127*, 10089−10095.
(23) Ashton, P. R.; Fyfe, M. C. T.; Hickingbottom, S. K.; Stoddart, J. F.; White, A. J. P.; Williams, D. J. *J. Chem. Soc., Perkin Trans. 2* **1998**, 2117−2128.